

The Influence of Thermal Radiation on Mixed Convection MHD Flow of a Casson Nanofluid over an Exponentially Stretching Sheet

T. Gangaiah^{1*}, N. Saidulu² and A. Venkata Lakshmi³

¹Department of Mathematics, Government Degree College, Mancherial, 504208, India.

²Department of Mathematics, Osmania University, Hyderabad, 500007, India.

³Department of Mathematics, UCT, Osmania University, Hyderabad, 500007, India.

(*) Corresponding author: tgangaiah79@gmail.com

(Received: 06 June 2018 and Accepted: 02 October 2018)

Abstract

The present article describes the effects of thermal radiation and heat source/sink parameters on the mixed convective magnetohydrodynamic flow of a Casson nanofluid with zero normal flux of nanoparticles over an exponentially stretching sheet along with convective boundary condition. The governing nonlinear system of partial differential equations along with boundary conditions for this fluid flow converted to a system of nonlinear ordinary differential equations by using appropriate similarity transformations. The converted system of equations were solved numerically by using Runge-Kutta fourth order method with shooting technique. The influence of various non-dimensional governing parameters on velocity, temperature and nanoparticle volume fraction profiles have been discussed and presented graphically. Furthermore, the impacts of these parameters on skin friction coefficient and local Nusselt number are exhibited graphically and analyzed. It found that the velocity profiles and skin friction coefficient increases with an increase in the mixed convection parameter whereas, an opposite trend observed with Casson fluid parameter and magnetic field parameter. The thermal boundary layer thickness enhanced with an increase in Biot number, magnetic field parameter, radiation parameter and heat source/sink parameter. Also, the local Nusselt number decreases with an increase in radiation parameter and heat source/sink parameter.

Keywords: Thermal radiation, Heat source/sink, Mixed convection, Casson nanofluid, Exponential stretching.

1. INTRODUCTION

The study of heat and mass transfer of the laminar boundary layer flow over a stretching sheet has expedited development due to its numerous applications in different engineering and industrial manufacturing processes like aerodynamics, wire drawing, hot rolling, extrusion of plastic and rubber sheets, glass blowing, condensation process of metallic plates, fiber spinning and many others. During such processes, both stretching and simultaneous cooling or heating have a decisive influence on the quality of the final products. The study of boundary layer flow over a continuous stretching surface with constant velocity was initiated by Sakiadis [1]. Later, Crane

[2] extended this concept to study two-dimensional viscous fluid flow in which velocity varies over a linearly stretching sheet and obtained a similar solution. Wang [3] enlarged this concept for three-dimensional flow and found exact similarity solution for the Navier-Stokes equations. The influence of suction/blowing on heat and mass transfer over a stretching sheet was studied by Gupta and Gupta [4]. The problems of Sakiadis and Crane were extended by many researchers like Carragher and Crane [5], Bidin and Nazar [6], Bhattacharyya et al. [7] and Sandeep and Sugunamma [8] under various stretching sheets and boundary conditions.

The magnetohydrodynamic (MHD) flow of an electrically conducting fluid has gained considerable interest in modern metallurgical and biomedical field. The process of coating of metals, MHD power generation systems, cooling of nuclear reactor, wound healing and MRI (Magnetic Resonance Imaging) to diagnose disease and surgical procedures are good examples of such fields. The Lorentz force interacts with the buoyancy force in governing the flow and temperature fields. Andersson [9] explained the exact solution of the Navier-Stokes equations for MHD flow. Some important literature on MHD steady flow and heat transfer on sliding plate can be found in Makinde [10]. Mahapatra et al. [11] investigated the steady magnetohydrodynamic stagnation point flow of power-law fluid over stretching surface. Furthermore, Ishak et al. [12], Akbar et al. [13], Madhu and Kishan [14], Ijaz et al. [15] and Anantha et al. [16] were made to examine the effects of MHD flow over various stretching sheets under different aspects.

An extensive research has been conducted on boundary layer flow which is caused by an exponentially stretching sheet due to its wider applications in technology. For instance, in the case of annealing and tinning of copper wires the final product depends on the variations of stretching velocity and temperature distribution. In such processes, both the kinematics of stretching and the simultaneous heating or cooling has a remarkable influence on the quality of the final outputs. Magyari and Keller [17] were the first to study the heat and mass transfer in the boundary layers flow over an exponentially stretching sheet. Elbashbeshy [18] studied the flow past an exponentially stretching surface. The effects on thermal boundary layer of MHD flow over an exponential stretching surface investigated by Odad et al. [19]. Recently, Mukhopadhyay [20], Rudraswamy and Gireesha [21], Hayat et al. [22] and Gangaiah et al. [23] investigated

various effects of heat and mass transfer over an exponentially stretching sheet.

The term nanofluid was proposed by Choi referring to dispersions of nanoparticles (10^{-9} mtr) in the base fluids such as water, ethylene glycol, and propylene glycol. Choi [24] showed that the addition of a small amount (less than 1 percent by volume) of nanoparticles to conventional heat transfer liquids increased the thermal conductivity of the fluid up to approximately two times. Masuda et al. [25] observed that the nanofluid enhances the thermal conductivity of the fluid flow. Buongiorno [26] noticed that Brownian diffusion and thermophoresis force are the main reasons behind the enhancement in heat transfer for nanofluid. Nield and Kuznetsov [27] studied analytically how the thermal instability in a porous medium layer saturated by a nanofluid. Angayar-kanni and Philip [28] reviewed on thermal properties of nanofluids. Thereafter, Sheikholeslami [29], Reddy and Naikoti [30], Ramya et al. [31] and many other researchers investigated on the MHD flow of nanofluid over an exponentially stretching sheet under various physical phases.

To understand the nature of real life fluids like shampoos, paints, blood, condensed milk and printing ink it is necessary to study non-Newtonian fluids. The complex nature of non-Newtonian fluids presents a challenge to physicists and mathematicians. In the recent past, the study of non-Newtonian fluid flow over a stretching surface has become a field of active research due to its widespread applications in technology and industry. For instance, polymer extrusion in the plastic processing industries, wire drawing, petroleum production, glass blowing, paper production, artificial fibers, hot rolling, cooling of metallic sheets or electronic chips and many others. The Power-law fluid, tangent hyperbolic fluid, Jeffrey fluid, Casson fluid, Williamson fluid, Rivlin-Ericksen fluid are some types in non-Newtonian fluids. In such fluids

Casson fluid is a non-Newtonian fluid which exhibits yield stress. Casson [32] presented a visco-elastic fluid model, later it is known as Casson fluid model. Dash et al. [33] defined Casson fluid as a shear thinning liquid which is assumed to have an infinite viscosity at zero rate of shear, a yield stress below which has no flow occurs and a zero viscosity at an infinite rate of shear. Fredrickson [34] investigated the kinematics of deformation and flow behaviour of Casson fluid in a tube. Charm and Kurland [35] and Walwander et al. [36] performed on blood with varying haematocrits, anticoagulants and temperatures and strongly suggested that the behaviour of blood as a Casson fluid. Malik et al. [37] explained the behaviour of Casson nanofluid over vertically exponentially stretching cylinder. Recently, Prabhakar and Shankar [38], Arthur et al. [39], Raju [40], Anantha et al. [41] and Tamoor [42] are also very keenly discussed the nature of Casson fluid under various stretching surfaces with various boundary conditions.

Over the last few years, a considerable amount of experimental and theoretical work has been carried out to determine the effects of heat generation/absorption on the heat and mass transfer. Cooling of electronic equipment, hot spot/sink modification of polymer manufacture, cooling/heating of plastic products etc. are good examples of applications of heat source/sink. On the other hand, the effects of thermal radiation on heat and mass transfer of various fluids over a stretching surface have significant importance due to its wider applications in physics, engineering and space technology. For example, thermal radiation effects may play an important role in controlling heat transfer in polymer processing industry. Nuclear power plants, high-temperature plasmas, cooling of nuclear reactors, liquid metal fluids, MHD accelerators, satellites and space vehicles are some important applications of radiative heat transfer. Pramanik [43] explained the thermal

radiation effects on Casson fluid over a porous stretching surface. Hayat et al. [44] examined the effects of chemical reaction and heat source/sink on mixed convection Casson nanofluid flow over a stretching surface. Bhattacharya et al. [45] derived an exact solution for Casson fluid flow over a permeable shrinking sheet with radiation effects. In the recent past, several works of literature Anki Reddy [46], Kumar et al. [47], Zia et al. [48] and Laxmi et al. [49] explained the influences of thermal radiation and heat source/sink on the MHD flow of various fluids over various stretching sheets under different boundary conditions.

The main aim of the present study is to describe the effects of mixed convection MHD flow of Casson fluid with zero normal flux of nanoparticles over an exponentially stretching sheet in presence of radiation and heat source/sink parameters along with the convective boundary condition. To get rid of gravitational effects at the surface of the sheet, we considered zero normal flux of nanoparticles in the fluid which is defined in boundary conditions. The present paper is organized as follows: Section 2 deals with the fluid flow model and how the governing non-linear partial differential equations are converted into non-linear ordinary differential equations is described in Sec. 3, method of solution. Section 4 (numerical method) explains, how we solved the resulting system of ODE with boundary conditions using Runge-Kutta method with shooting technique. In Section 5, we analyzed both the numerical and graphical results. The conclusions of this paper are presented in Section 6.

2. MATHEMATICAL MODELING

Consider the steady, two-dimensional mixed convection boundary layer incompressible, laminar flow of magnetohydrodynamic Casson fluid with zero normal flux of nanoparticles over an exponentially stretching sheet with thermal radiation and heat source/sink. A variable

magnetic field $B(x)$ (normal to the surface) with suction and convective heat conditions are applied at the surface of the sheet. The rheological equation of state for an isotropic and incompressible flow of a Casson fluid can be written as [39, 44]:

$$\tau_{ij} = \begin{cases} 2(\mu_B + P_y / \sqrt{2\pi})e_{ij}, & \pi > \pi_c \\ 2(\mu_B + P_y / \sqrt{2\pi_c})e_{ij}, & \pi < \pi_c \end{cases} \quad (1)$$

where μ_B is plastic dynamic viscosity of non-Newtonian fluid, P_y is the yield stress of the fluid, π is the product of the component of the deformation rate with itself, here $\pi = e_{ij} \cdot e_{ij}$, and e_{ij} is the $(i, j)^{\text{th}}$ component of the deformation rate and π_c is the critical value of π based on the non-Newtonian model.

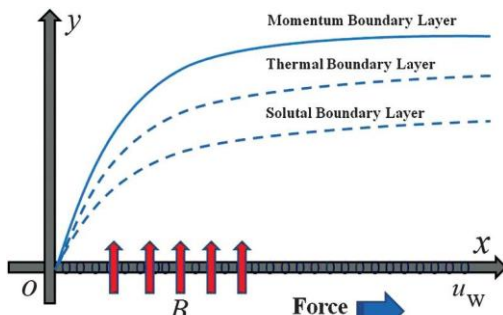


Figure 1. Flow configuration and coordinate system.

The flow is assumed to be generated by linear stretching of the sheet from a slit with a large force such that the velocity of the sheet is an exponential order, caused by the simultaneous application of two equal and opposite forces along the x-axis. The x-axis is taken as the stretching surface in the direction of the fluid flow while the y-axis is perpendicular to it. The flow is coinciding with the plane $y=0$ and is confined to $y>0$. Keeping the origin fixed the sheet is then stretched with a velocity (U_w) varying linearly with the distance from the slit and T_f as the temperature at the surface. The mass flux of the nanoparticle at the wall is assumed to be zero. A variable magnetic field $B = B_0 e^{\frac{x}{2L}}$

is applied to the sheet, where B_0 is the initial strength of the magnetic field. By all these considerations the governing equations of continuity, momentum, energy and concentration for this flow are given as follows [39, 44]:

$$\frac{\partial u}{\partial x} + \frac{\partial v}{\partial y} = 0, \quad (2)$$

$$u \frac{\partial u}{\partial x} + v \frac{\partial u}{\partial y} = \nu(1 + \frac{1}{\beta}) \frac{\partial^2 u}{\partial y^2} + g \beta_t (T - T_\infty) + g \beta_c (C - C_\infty) - \frac{\sigma B^2 u}{\rho}, \quad (3)$$

$$u \frac{\partial T}{\partial x} + v \frac{\partial T}{\partial y} = \frac{k}{\rho c_p} \frac{\partial^2 T}{\partial y^2} + \frac{Q}{\rho c_p} (T - T_\infty) - \frac{1}{\rho c_p} \frac{\partial q_r}{\partial y} + \tau \left[D_B \frac{\partial C}{\partial y} \frac{\partial T}{\partial y} + \frac{D_T}{T_\infty} \left(\frac{\partial T}{\partial y} \right)^2 \right], \quad (4)$$

$$u \frac{\partial C}{\partial x} + v \frac{\partial C}{\partial y} = D_B \frac{\partial^2 C}{\partial y^2} + \frac{D_T}{T_\infty} \frac{\partial^2 T}{\partial y^2} \quad (5)$$

The boundary conditions associated with the problem are:

$$u = U_w, v = V_w, \frac{\partial T}{\partial y} = -\frac{h_f}{k} (T_f - T), \quad (6)$$

$$D_B \frac{\partial C}{\partial y} + \frac{D_T}{T_\infty} \frac{\partial T}{\partial y} = 0 \text{ at } y = 0 \text{ and}$$

$$u \rightarrow 0, T \rightarrow T_\infty, C \rightarrow C_\infty \text{ as } y \rightarrow \infty$$

In the above equations, u and v are velocity components in the x and y directions respectively, $\nu = \frac{\mu}{\rho}$ is the kinematic viscosity, μ is the coefficient of the viscosity, ρ is the density of the fluid,

$\beta = \mu_B \frac{\sqrt{2\pi_c}}{P_y}$ is the Casson fluid parameter, g is the gravitational acceleration, β_t is the thermal expansion coefficient, T is the temperature of the fluid, T_∞ is the ambient fluid temperature, β_c is the concentration expansion coefficient, C is the concentration of the fluid, C_∞ is the ambient fluid concentration, σ is the electrical conductivity, k is thermal conductivity and c_p is the specific heat of

the fluid at constant pressure, q_r is the radiative heat flux, $Q = Q_0 e^{\frac{x}{2L}}$ is the heat generation/absorption parameter which may take on either positive (heat source when $Q > 0$) or negative (heat sink when $Q < 0$) value, Q_0 is a constant, $\tau = \frac{(\rho c)_p}{(\rho c)_f}$ is the ratio of the effective heat capacity of the nanoparticles material to the heat capacity of the base fluid, D_B is the Brownian diffusion coefficient and D_T is the thermophoresis diffusion coefficient. Also, $U_w = U_0 e^{\frac{x}{L}}$ is the stretching velocity, U_0 is the reference velocity, L is the characteristic length, $V_w = -v_0 e^{\frac{x}{2L}}$ is a special type of velocity on the wall, where v_0 is the initial strength of the suction, $V_w > 0$ is the velocity of suction and $V_w < 0$ is the velocity of blowing h_f is the convective heat transfer coefficient and T_f is the hot fluid temperature at the sheet.

By Roseland approximation for radiation [50, 51], the radiative heat flux q_r is simplified as

$$q_r = -\frac{4\sigma^*}{3k^*} \frac{\partial T^4}{\partial y}. \quad (7)$$

Here σ^* is the Stefan-Boltzmann constant and k^* is the absorption coefficient. Assume that the temperature differences, such as the term T^4 within the flow, may be expressed as a linear function of temperature. After neglecting higher-order terms in Taylor's series expansion for T^4 about T_∞ we have

$$T^4 \cong 4T_\infty^3 T - 3T_\infty^4. \quad (8)$$

By using eqns. (7) and (8), we get,

$$q_r = -\frac{16\sigma^* T_\infty^3}{3k^*} \frac{\partial T}{\partial y} \quad (9)$$

3. METOD OF SOLUTION

To scrutinize the problem, we introduce the following similarity transformations to derive a system of ordinary differential equations from the given system of non-linear partial differential equations.

$$\eta = \sqrt{\frac{U_0}{2\nu L}} e^{\frac{x}{2L}} y, \quad \psi = \sqrt{2U_0\nu L} e^{\frac{x}{2L}} f(\eta), \\ \theta(\eta) = \frac{T - T_\infty}{T_f - T_\infty}, \quad \phi(\eta) = \frac{C - C_\infty}{C_\infty}. \quad (10)$$

where η is the similarity variable, $\psi(x, y)$ is the stream function, $f(\eta), \theta(\eta)$ and $\phi(\eta)$ are dimensionless stream, temperature and concentration functions respectively. The equation of continuity is satisfied by choosing $\psi(x, y)$ such that

$$u = \frac{\partial \psi}{\partial y}, \quad v = -\frac{\partial \psi}{\partial x}. \quad \text{And hence}$$

$$u = U_0 e^{\frac{x}{L}} f', \quad v = -\sqrt{\frac{U_0\nu}{2L}} e^{\frac{x}{2L}} (\eta f' + f).$$

By substituting the above transformations, the equations (3) - (5) can be transformed into the system of ordinary differential equations

$$(1 + \frac{1}{\beta}) f''' + ff'' - 2(f')^2 - M f' \\ + \lambda(\theta + N\phi) = 0, \quad (11)$$

$$\frac{1}{Pr}(1 + \frac{4R}{3})\theta'' + \theta' f + Q_H \theta \\ + Nb(\theta' \phi') + Nt(\theta')^2 = 0, \quad (12)$$

$$\phi'' + Sc \phi' f + \frac{Nt}{Nb} \theta'' = 0 \quad (13)$$

The corresponding dimensionless boundary conditions (6) become

$$f(\eta) = S, \quad f'(\eta) = 1, \quad \theta'(\eta) = Bi [\theta(0) - 1], \\ \phi'(\eta) = -\frac{Nt}{Nb} \theta'(\eta) \quad \text{at } \eta = 0 \text{ and} \\ f'(\eta) \rightarrow 0, \theta(\eta) \rightarrow 0, \phi(\eta) \rightarrow 0 \text{ as } \eta \rightarrow \infty \quad (14)$$

Here the primes denote differentiation with respect to η , $\lambda = \frac{2Lg\beta_t(T_f - T_\infty)}{U_w^2}$ is the mixed convection parameter,

$N = \frac{\beta_c C_\infty}{\beta_i (T_f - T_\infty)}$ is the concentration

buoyancy parameter, $M = \frac{2L\sigma B_0^2}{U_0 \rho}$ is the

magnetic field parameter, $Pr = \frac{\mu c_p}{k} = \frac{\nu}{\alpha}$

is the Prandtl number, $R = \frac{4\sigma^* T_\infty^3}{kk^*}$ is the

radiation parameter, $Q_H = \frac{2LQ_0}{U_0 \rho C_p}$ is the

heat source/sink parameter, $Nb = \frac{\tau D_B C_\infty}{\nu}$

is the Brownian motion parameter,

$Nt = \frac{\tau D_T (T_f - T_\infty)}{\nu T_\infty}$ is the thermophoresis

parameter, $Sc = \frac{\nu}{D_B}$ is the Schmidt

number, $S = v_0 \sqrt{\frac{2L}{\nu U_0}} > 0$ is the suction

parameter and $Bi = \frac{h_f}{k} \sqrt{\frac{2L\nu}{U_w}}$ is the Biot

number.

The parameters of physical interest in this problem are the skin friction coefficient C_{f_x} and the local Nusselt number Nu_x which represents the wall shear stress and the wall heat flux respectively and defined as

$$C_{f_x} = \frac{\tau_w}{\rho U_w^2}, \quad Nu_x = \frac{x q_w}{k(T_f - T_\infty)}.$$

Here $\tau_w = \mu \left(1 + \frac{1}{\beta}\right) \left[\frac{\partial u}{\partial y} \right]_{y=0}$ is the wall

shear stress and $q_w = -k \left(1 + \frac{4R}{3}\right) \left[\frac{\partial T}{\partial y} \right]_{y=0}$

is the wall heat flux. After using similarity transformations mentioned in Eqn. (10), the skin friction coefficient and the local Nusselt number are transformed to

$$(Re_x)^{\frac{1}{2}} C_{f_x} = \sqrt{\frac{x}{2L}} \left(1 + \frac{1}{\beta}\right) f''(0), \quad (15)$$

$$(Re_x)^{\frac{-1}{2}} Nu_x = -\sqrt{\frac{x}{2L}} \left(1 + \frac{4R}{3}\right) \theta'(0). \quad (16)$$

Here $Re_x = \frac{x U_w}{\nu}$ is the local Reynolds number.

4. NUMERICAL METHOD

The system of equations (11) - (13) along with the boundary conditions (14) are highly non-linear ordinary differential equations and hence unable to solve analytically. In order to solve these equations numerically, we used Runge-Kutta fourth order method with shooting technique which is described by Dulal [52]. Here it is important to choose the appropriate finite values in boundary conditions for $\theta(\eta)$ and $\theta'(\eta)$ at $\eta = 0$. In order to determine the value of η_∞ , we start with some initial guess value for some particular set of physical parameters to obtain the values of $f''(0)$ and $\theta'(0)$.

Firstly, we use the following set of variables to reduce the above set of differential equations (11) - (13) into a system of first-order differential equations

$$f = f_1, \quad f' = f_2, \quad f'' = f_3, \quad (17)$$

$$\theta = f_4, \quad \theta' = f_5, \quad \phi = f_6, \quad \phi' = f_7.$$

Re-write the equations (11) - (13) with these variables, we get the system of first-order differential equations as below:

$$f'_1 = f'_2 = f_2, \quad (18)$$

$$f'_2 = f'' = f_3, \quad (19)$$

$$f'_3 = f''' = \frac{1}{(1 + \frac{1}{\beta})} [2(f_2)^2 + M f_2 - f_1 f_3 - \lambda(f_4 + N f_6)], \quad (20)$$

$$f'_4 = \theta' = f_5, \quad (21)$$

$$f'_5 = \theta'' = \frac{-Pr}{(1 + \frac{4R}{3})} [f_1 f_5 + Q_H f_4 + Nb f_5 f_7 + Nt(f_5)^2], \quad (22)$$

$$f'_6 = \phi' = f_7, \quad (23)$$

$$f_7' = \phi'' = -Sc f_1 f_7 + \frac{Nt}{Nb} \frac{Pr}{(1+\frac{4R}{3})} [f_1 f_5 + Q_H f_4 + Nb f_5 f_7 + Nt(f_5)^2] \quad (24)$$

The boundary conditions are modified as

$$f_1(\eta) = S, f_2(\eta) = 1, f_5(\eta) = Bi(f_4(\eta) - 1), \\ f_7(\eta) = \frac{-Nt}{Nb} f_5(\eta) \text{ at } \eta = 0 \text{ and} \\ f_2(\eta) \rightarrow 0, f_4(\eta) \rightarrow 0, f_6(\eta) \rightarrow 0 \text{ as } \eta \rightarrow \infty$$

In order to solve the system of equations (18) - (25) along with the boundary conditions, we require a value for $\theta(0) = f_4(0)$ and $\theta'(0) = f_5(0)$. But no such value is given at the boundary. Hence suitable guess functions are chosen for $f(\eta)$, $\theta(\eta)$ and $\phi(\eta)$ to calculate the values of $\theta(0)$, $\theta'(0)$ in MATLAB algorithm for the Runge-Kutta method with shooting technique with step size $\Delta\eta = 0.01$. We choose the values for $\eta_{max} = 10$, $\theta(0) = 2$, $\theta'(0) = -1$ and compared the calculated numerical values of $-\theta'(0)$ with the existing results. The above procedure is repeated until we get the converged results within a tolerance limit 10^{-4} .

5. RESULTS AND DISCUSSION

To study the behaviour of velocity, temperature and nanoparticle volume fraction profiles along with physical quantities wall shear stress and heat transfer rate for various values of the governing parameters namely, Casson fluid parameter (β), mixed convection parameter (λ), concentration buoyancy parameter (N), magnetic field parameter (M), Prandtl number (Pr), radiation parameter (R), heat source/sink parameter (Q_H), Brownian motion parameter (Nb), thermophoresis parameter (Nt), suction parameter (S) and the Biot number (Bi), we used MATLAB programme for Runge-

Kutta fourth order method with shooting technique and computed the numerical computations. The results are reported in terms of Table 1 and graphs as shown in Figs. [2-27]. It is found that the obtained results are in excellent agreement with previous results. Throughout the study, for numerical results and plotting graphs we used $\beta = 0.5$, $\lambda = 0.3$, $M = 0.3$, $Pr = 0.72$, $R = 0.3$, $Q_H = 0.2$, $Sc = 0.6$, $Nt = Nb = 0.2$, $S = 0.3$ and $Bi = 0.2$ except the varied values in respective figures and tables.

Table 1. Comparison of Nusselt number $[-\theta'(0)]$ for various values of β , Nt and Nb when $M = R = Q_H = S = 0$; $\lambda = N = 0.3$; $Bi = 0.2$; $Sc = 0.7$

β	Nt	Nb	Hayat [44]	Present values
0.5	0.2	0.2	0.15271	0.15281
0.7			0.15204	0.15197
0.9			0.15150	0.15146
0.5	0.4		0.15195	0.15207
	0.6		0.15106	0.15114
0.5	0.2	0.4	0.15186	0.15180
		0.6	0.15100	0.15109

To verify the accuracy of the applied numerical scheme, we compared the values of local Nusselt Number $[-\theta'(0)]$ for various values of β, Nt, Nb with the existing results of Hayat et al. [44] in Table 1 in absence of magnetic field, thermal radiation, heat source/sink, suction and the fixed values for the parameters $N = \lambda = 0.3$, $Pr = 1$, $Bi = 0.2$ and $Sc = 0.7$. The results are found in good agreement with small variation due to boundary conditions.

5.1. Velocity Profiles

To visualize the results, here we discussed the graphical outcomes of the problem in a physical sense. The influences of Casson fluid parameter (β), mixed convection parameter (λ), concentration buoyancy parameter (N),

magnetic field parameter (M) and suction parameter (S) on the dimensionless velocity profiles are plotted in Figures [2 - 6] respectively. It is clear from the Fig. 2 that, an increase in Casson fluid parameter β reduces the velocity boundary layer.

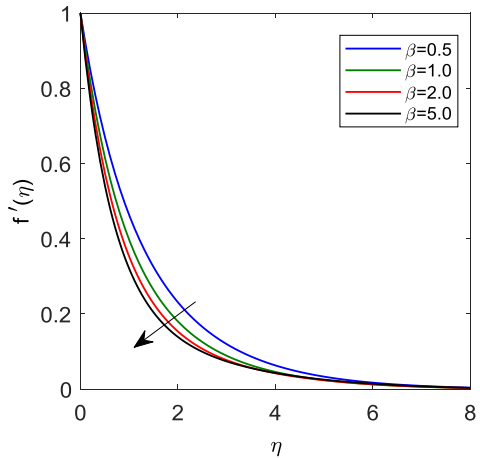


Figure 2. Influence of Casson fluid parameter β on velocity profiles.

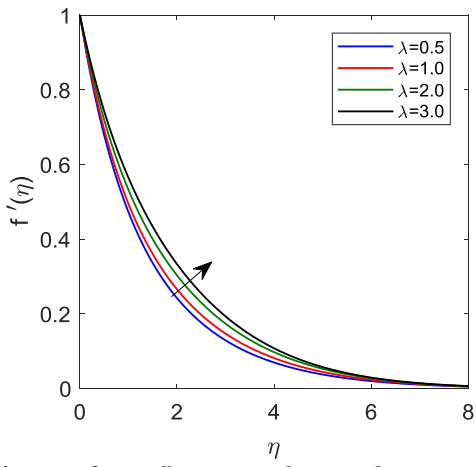


Figure 3. Influence of mixed convection parameter λ on velocity profiles.

Due to the increase in β , increases the plastic dynamic viscosity of the fluid which increases the internal resistance of the fluid and hence reduces the velocity profiles of the fluid. Fig. 3 shows that the velocity profiles increase with the increase in mixed convection parameter (λ). The increase in mixed convection parameter has the tendency to increase the thermal buoyancy effects which acts like favorable

pressure gradient and accelerates the fluid flow, so the velocity boundary layer thickness increases with the increase in λ .

The effects of concentration buoyancy parameter N on velocity profiles as depicted in Fig. 4. The similar explanation may present for the concentration buoyancy parameter behavior, so the velocity of the fluid enhances with an increase in ' N '.

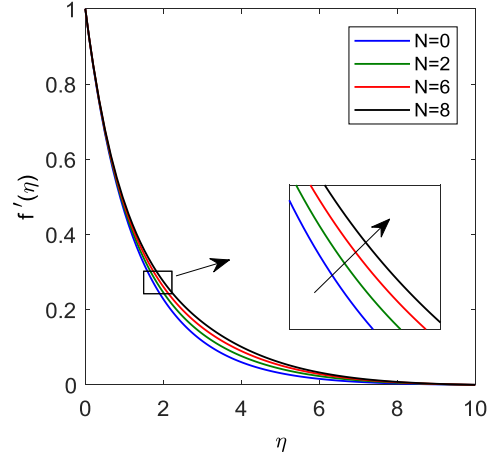


Figure 4. Influence of concentration buoyancy parameter N on velocity profiles.

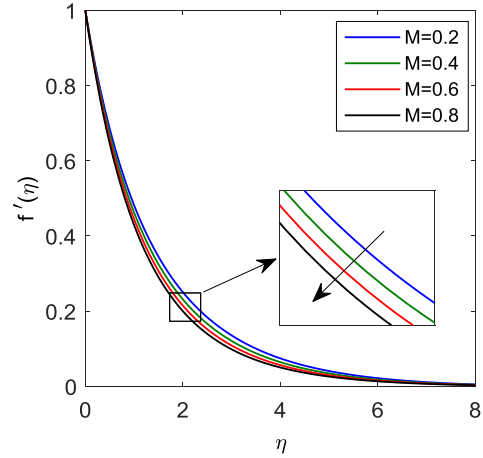


Figure 5. Influence of magnetic field parameter M on velocity profiles.

Fig. 5 concludes that an increase in the magnetic field parameter M decreases the transport process. Due to the increase in ' M ' produces a force which called as Lorentz force and the increase in that force produces much more resistance to the fluid. Hence the velocity of the fluid decreases with an increase in M . It is

evident from the Fig. 6 that an increase in suction parameter (S) decreases the velocity of the fluid. Due to the suction, the fluid brought close to the sheet, so increases resistivity and hence reduces the velocity boundary layer thickness.

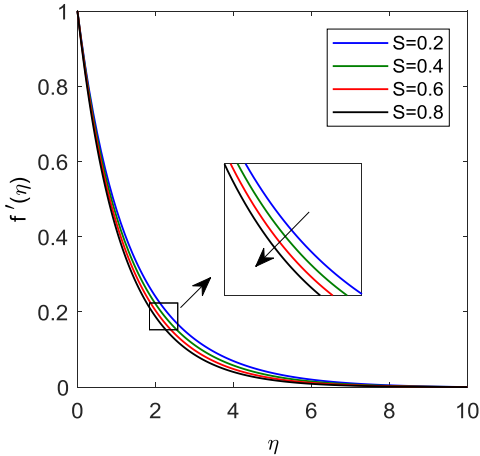


Figure 6. Influence of suction parameter S on velocity profiles.

5.2. Temperature Profiles

Figures [7 – 16] depicts the effects of the various dimensionless parameters on thermal boundary layer. It is clear from the Fig. 7 that, an increase in suction parameter (S) shrinking the thermal boundary layer thickness. Since increase in suction cool down the layers of fluid flow and hence decreases the temperature profiles. The variation of a magnetic fluid parameter (M) on temperature profiles plotted in Fig. 8. Noticed that, an increase in M increases strong Lorentz force and hence increases thermal boundary layer thickness. An opposite trend observed in Fig. 9, the increase in Prandtl number (Pr) with temperature profiles. The enhancement in Pr decreases the thermal diffusivity and hence reduces the thermal boundary layer thickness. The impact of mixed convection parameter (λ) on thermal boundary layer thickness is visualized in Fig. 10. Since the increase in λ , increases the buoyancy force which has the tendency to induce more flow along the surface at the expense of small reductions in the temperature profile.

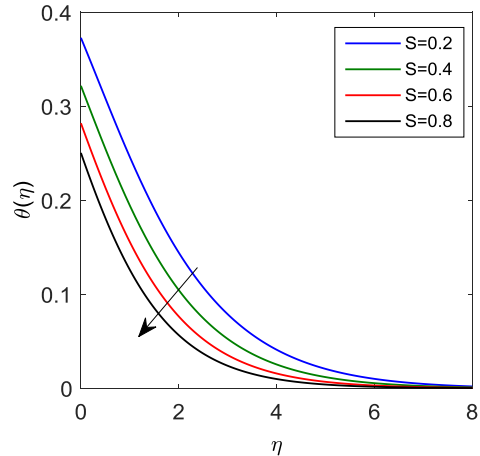


Figure 7. Influence of suction parameter S on temperature profiles.

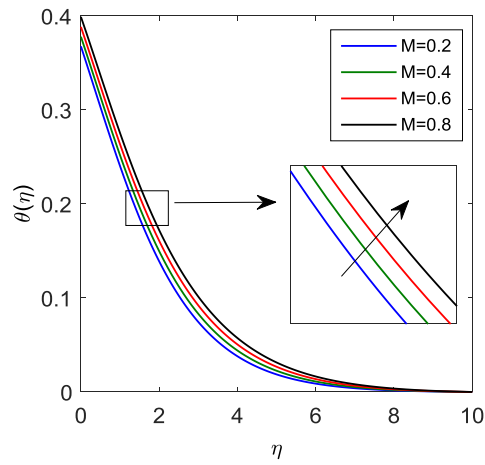


Figure 8. Influence of magnetic field parameter M on temperature profiles.

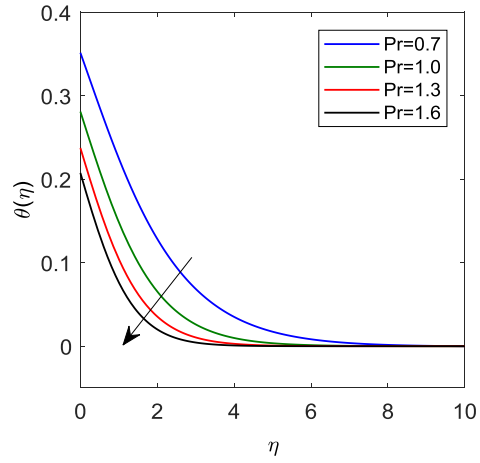


Figure 9. Influence of Prandtl number Pr on temperature profiles.

The impact of concentration buoyancy parameter (N) on temperature profiles is as depicted in Fig. 11. It illustrates that an

increase in ' N ' reduces the thermal buoyancy force and hence the temperature.

The influence of radiation parameter (R) on the thermal boundary layer is plotted in fig. 12 and noticed that the increase in R increases the radiative heat flux which enhances the thermal boundary layer of the

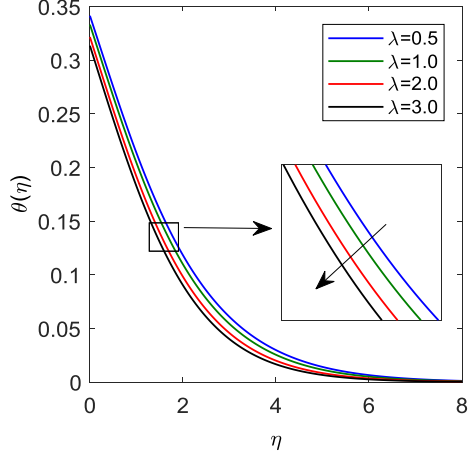


Figure 10. Influence of mixed convection parameter λ on temperature profiles.

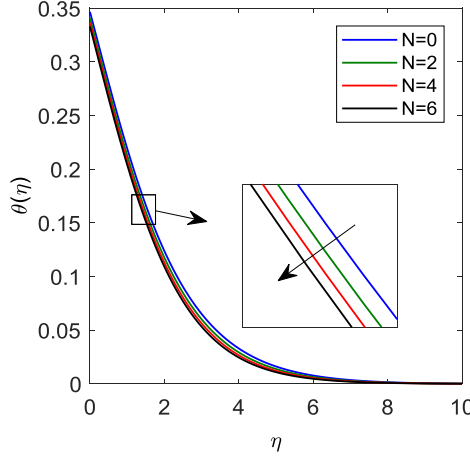


Figure 11. Influence of concentration buoyancy parameter N on temperature profiles

fluid. From Fig. 13, increase in heat source/sink parameter (Q_H) increases the thermal boundary layer thickness. In fact, an increase in Q_H leads to higher temperature field in the thermal boundary layer of the field. It is observed from Fig. 14 that, an increase in Brownian motion parameter Nb increase the temperature of the fluid.

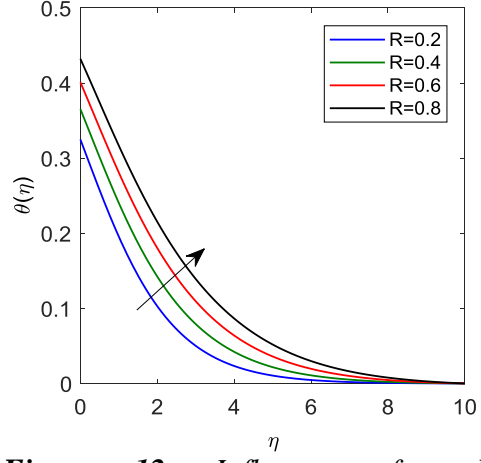


Figure 12. Influence of radiation parameter R on temperature profiles.

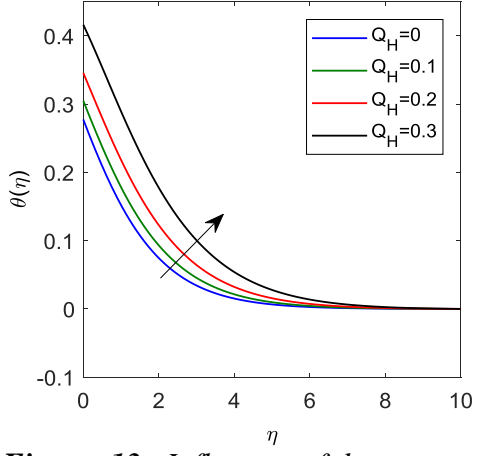


Figure 13. Influence of heat source/sink parameter Q_H on temperature profiles.

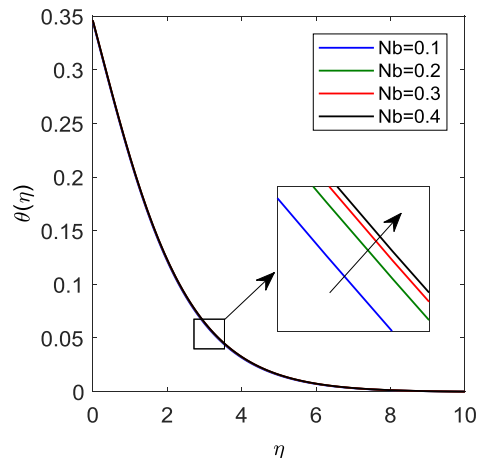


Figure 14. Influence of Brownian motion parameter Nb on temperature profiles.

Due to Brownian motion, more collisions with fast-moving atoms in the fluid take place and hence increases the kinetic

energy of the particles suspended in the fluid. Fig. 15 reveals that thermophoresis parameter Nt enhances the temperature profiles of the fluid with an increase in Nt . The enhancement of thermophoresis force moves the nanoparticles from the hot surface to the cold one and hence the temperature of the fluid increases with Nt . The effect of Biot Number Bi on temperature profiles exhibited in Fig. 16. Since 'Bi' is the dimensionless parameter and it gives the

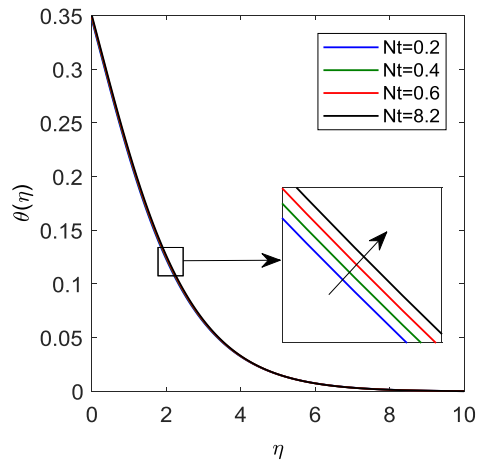


Figure 15. Influence of thermophoresis parameter Nt on temperature profiles.

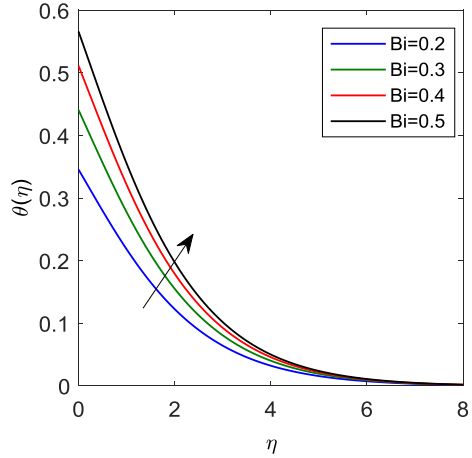


Figure 16. Influence of Biot number Bi on temperature profiles.

ratio of the heat transfer rate to the thermal conductivity. As an increase in Bi (small values of Bi) the heat flux is increased which leads to enhancing the temperature profiles.

5. 3. Concentration Profiles

The effects of various parameters on nanoparticle volume fraction profiles displayed in Figs. [17-21].

The influence of Biot number (Bi) on concentration profiles displayed in Fig. 17. It can be seen from the figure that, a rise in the ' Bi ' increases convective mass transfer coefficient of the fluid as an effect of that it increases the concentration boundary layer thickness.

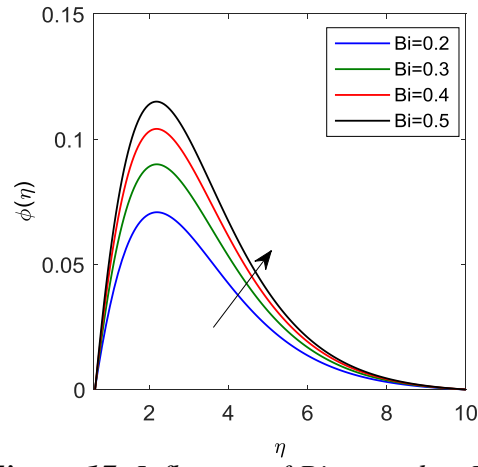


Figure 17. Influence of Biot number Bi on nanoparticle volume fraction profiles.

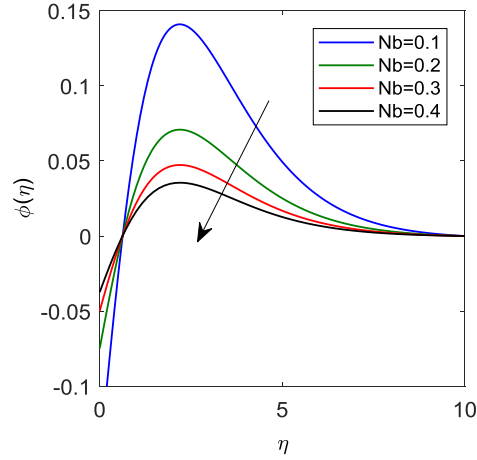


Figure 18. Influence of Brownian motion parameter Nb on nanoparticle volume fraction profiles.

The impact of Brownian motion parameter (Nb) on the concentration profile plotted in Fig. 18. Due to the increase in Nb , the Brownian motion takes place and increases diffusion of the fluid. As a result, the concentration boundary layer thickness decreases. Fig. 19 shows the effect of thermophoresis parameter (Nt)

on concentration profiles. With an increase in Nt , increases thermophoretic force which moves nanoparticles from hot region to cool region and consequently, it increases the concentration boundary layer thickness. The thickness of the concentration boundary layer significantly large for a slight increase in Nt . The effect of the Prandtl number Pr on the nanoparticle volume fraction depicted in Fig. 20. A small variation (initially increasing near the sheet and then decreasing away from the sheet) observed in the concentration boundary layer with the increase in the Prandtl number. The impacts of the Schmidt number (Sc) on nanoparticle volume fraction profile are displayed in Fig. 21. It reveals that, with an increase in ' Sc ' the mass diffusivity decreases and hence the concentration boundary layer thickness.

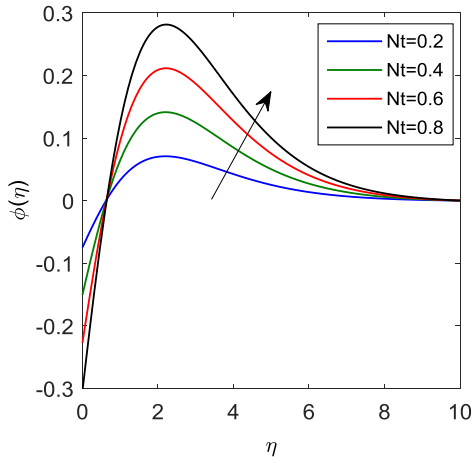


Figure 19. Influence of thermophoresis parameter Nt on nanoparticle volume fraction profiles.

Also, the figures 22 and 23 displays the variations of the local skin friction coefficient [C_{fx}] with various values of magnetic field parameter (M) for three different values of Casson fluid parameter (β) and mixed convection parameter (λ), respectively. It was found that skin friction coefficient C_{fx} increases with an increase in λ and reverse nature observed with

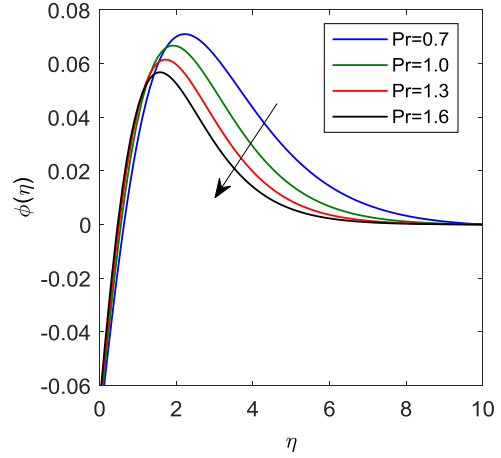


Figure 20. Influence of Prandtl number Pr on nanoparticle volume fraction profiles.

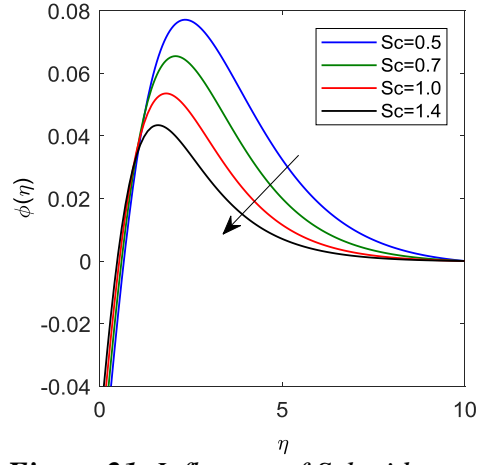


Figure 21. Influence of Schmidt number Sc on nanoparticle volume fraction profiles.

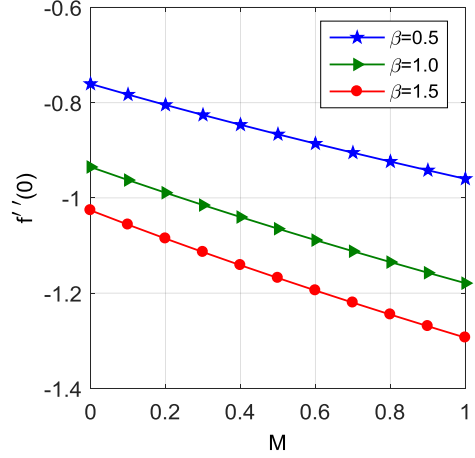


Figure 22. Effects of ' M ' and β on the skin friction coefficient.

both M and β . Figures 24 and 25 represent the behaviour of the local Nusselt number [$-\theta'(0)$] with thermophoresis parameter (Nt) for three different values of Biot number (Bi)

and Brownian motion parameter (Nb) respectively.

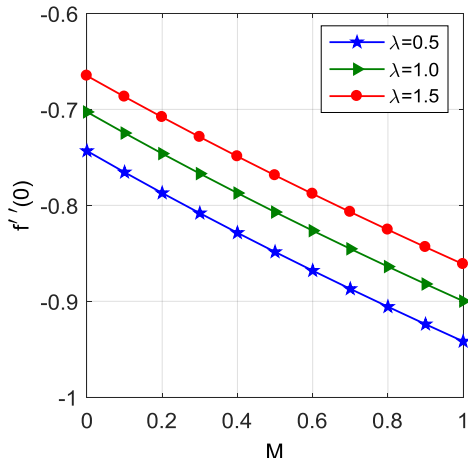


Figure 23. Effects of 'M' and λ on the skin friction coefficient.

It is clear from the figures that, the $[-\theta'(0)]$ value increase with the increasing values of 'Bi' and reverse trend observed with the increasing values of 'Nt' and 'Nb'.

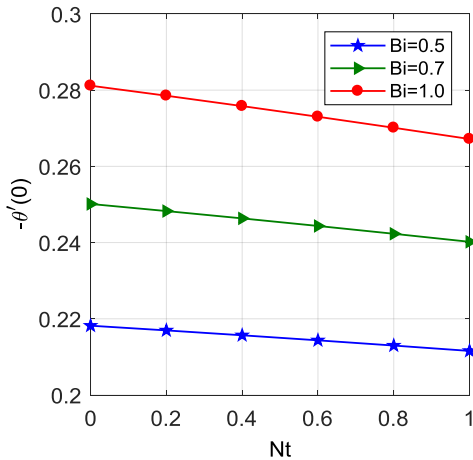


Figure 24. Effects of 'Nt' and 'Bi' on the local Nusselt number.

Figures 26 and 27 explains the change in local Nusselt number $[-\theta'(0)]$ with heat source/sink parameter (Q_H) for three different values of radiation parameter (R) and Prandtl number (Pr) respectively. As an increase in ' Q_H ' and ' R ' decrease the value of $[-\theta'(0)]$, whereas an increase in ' Pr ' increases the local Nusselt number. From these, we conclude that local Nusselt

number decreases with Nt , Nb , Q_H and R and it increases with Bi and Pr .

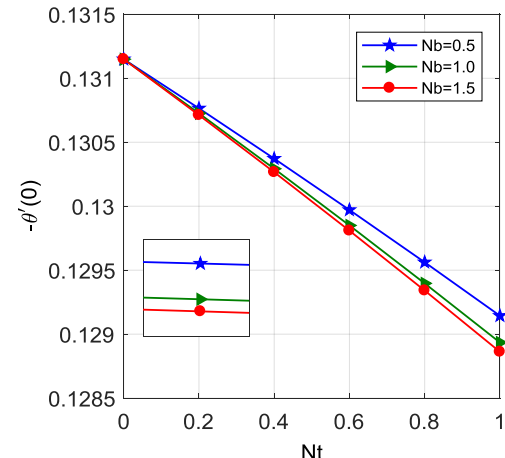


Figure 25. Effects of 'Nt' and 'Nb' on local Nusselt number.

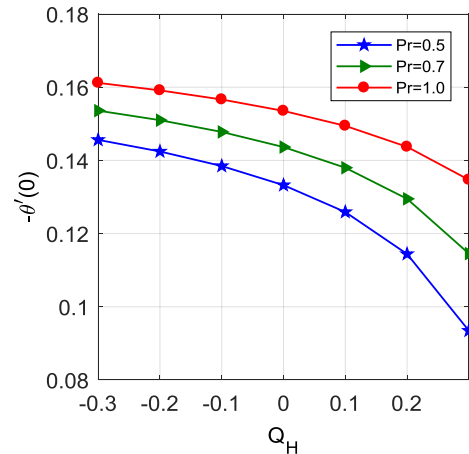


Figure 26. Effects of ' Q_H ' and ' Pr ' on the local Nusselt number.

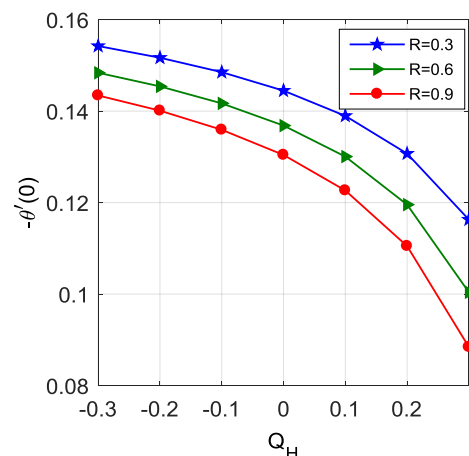


Figure 27. Effects of ' Q_H ' and ' R ' on the local Nusselt number.

6. CONCLUSIONS

The present study investigated the various effects of thermal radiation and heat source/sink parameters on the mixed convective MHD flow of Casson nanofluid with passive nanoparticles over an exponentially stretching sheet. MATLAB software was used for solving Runge-Kutta fourth order method with shooting technique and then analyzed numerically and graphically. The key findings of this paper are:

1. The velocity profile of the fluid enhances with the increasing values of mixed convection parameter and concentration buoyancy parameter while it decreases with an increase in the Casson fluid parameter, magnetic field parameter and suction parameter.
2. A rise in radiation parameter and heat source/sink parameters increases the thermal boundary layer thickness.
3. The temperature profiles of the fluid reduce with an increase in mixed convection parameter, suction parameter, Prandtl number and concentration buoyancy number.
4. An Increase in Brownian motion parameter, thermophoresis parameter, magnetic field parameter and Biot number

enhances the temperature profiles of the fluid.

5. The nanoparticle volume fraction profiles decrease with an increase in Brownian motion parameter, Prandtl number and Schmidt number and increase with thermophoresis parameter and Biot number.

6. The skin friction coefficient decreases with an increase in magnetic field parameter, Casson fluid parameter and increases with mixed convection parameter.

7. The local Nusselt number increases with an increase in Biot number and Prandtl number and reverse nature observed with thermophoresis parameter, Brownian motion parameter, radiation parameter and heat source/sink parameter.

ACKNOWLEDGEMENT

The authors wish to express their sincere thanks to the reviewers for their valuable comments and constructive suggestions to improve the quality of this article. The first author is very much thankful to the University Grants Commission, New Delhi, India, for providing an opportunity to do research work under Faculty Development Programme, UGC XII plan.

REFERENCES

1. Sakiadis, B. C., (1961). "Boundary layer behaviour on continuous solid surfaces, II. The boundary layer on a continuous flat surface", *AICHE Journal*, 7: 221-225.
2. Crane, L. J., (1970). "Flow past a stretching plate", *Zeitschrift für angewandte Mathematik und Physik*, 21(4): 645-647.
3. Wang, C. Y., (1984). "The three-dimensional flow due to a stretching flat surface", *The Physics of Fluids*, 27(8): 1915-1917.
4. Gupta, P. S., Gupta, A. S., (1977). "Heat and mass transfer on a stretching sheet with suction or blowing", *The Canadian journal of chemical engineering*, 55: 744-746.
5. Carragher, P., Crane, L. J., (1982). "Heat transfer on a continuous stretching sheet", *Zeitschrift für angewandte Mathematik und Physik*, 62: 564-565.
6. Bidin, B., Nazar, R., (2009). "Numerical solution of the boundary layer flow over an exponentially stretching sheet with thermal radiation", *European Journal of Scientific Research*, 33(4): 710-717.
7. Bhattacharyya, K., Mukhopadhyay, S., Layek, G.C., (2011). "Slip effects on boundary layer stagnation-point flow and heat transfer towards a shrinking sheet", *International Journal of Heat Mass Transfer*, 54(1-3): 308-313.
8. Sandeep, N., Sugunamma, V., (2014). "Radiation and inclined magnetic field effects on unsteady hydromagnetic free convection flow past an impulsively moving vertical plate in a porous medium", *Journal of Applied Fluid Mechanics*, 7(2): 275-286.
9. Andersson, H. I., (1995). "An exact solution of the Navier-Stokes equations for MHD flow", *Acta Mechanica*, 113: 241-244.
10. Makinde, O. D., (2001). "MHD steady flow and heat transfer on the sliding plate" *AMSE, Modelling, Measurement and Control B*, 70(1): 61-70.

11. Mahapatra, T. R., Nandy, S. K., Gupta, A. S., (2009). "Magnetohydrodynamic stagnation-point flow of a power-law fluid towards a stretching surface", *International Journal of Non-Linear Mechanics*, 44: 123-128.
12. Ishak, A., Bachok, N., Nazar, R., Pop, I., (2010). "MHD mixed convection flow near the stagnation-point on a vertical permeable surface", *Physica A: Statistical Mechanics and its Applications*, 389: 40-46.
13. Akbar, N. S., Ebai, A., Khan, Z. H., (2015). "Numerical analysis of magnetic field effects on Eyring-Powell fluid flow towards a stretching sheet", *Journal of magnetism and Magnetic Materials*, 382: 355-358.
14. Madhu, M., Kishan, N., (2016). "Magnetohydrodynamic mixed convection of a non-Newtonian power-law nanofluid past a moving vertical plate with variable density", *Journal of the Nigerian Mathematical Society*, 35: 199-207.
15. Ijaz Khan, M., Sumaira, Q., Hayat, T., Waqas, M., Imran Khan, M., Alsaedi, A., (2018), "Entropy generation minimization and binary chemical reaction with Arrhenius activation energy in MHD radiative flow of nanomaterial", *Journal of Molecular Liquids*, 259: 274-283.
16. Anantha Kumar, K., Ramana Reddy J. V., Sugunamma, V., Sandeep, N., (2018). "Magnetohydrodynamic Cattaneo-Christov flow past a cone and a wedge with variable heat source/sink", *Alexandria Engineering Journal*, 57: 435-443.
17. Magyari, E., Keller, B., (1999). "Heat and mass transfer in the boundary layers on an exponentially stretching continuous surface", *Journal of Physics D-Applied Physics*, 32(4): 577-585.
18. Elbashbeshy, E. M. A., (2001). "Heat transfer over an exponentially stretching continuous surface with suction", *Archive of Applied Mechanics*, 53: 643-651.
19. Al-Odat, M. Q., Damseh, R. A., Al-Azab, T. A., (2006). "Thermal boundary layer on an exponentially stretching continuous surface in the presence of magnetic field effect", *International Journal of Applied Mechanics and Engineering*, 11: 289-299.
20. Mukhopadhyay, S., (2013). "Slip effects on MHD boundary layer flow over an exponentially stretching sheet with suction/blowing and thermal radiation", *Ain Shams Engineering Journal*, 4(3): 485-491.
21. Rudraswamy, N. G., Gireesha, B. J., (2014). "Influence of chemical reaction and thermal radiation on MHD boundary layer flow and heat transfer of a nanofluid over an exponentially stretching sheet", *Journal of Applied Mathematics and Physics*, 2: 24-32.
22. Hayat, T., Waqas, M., Shehzad, S. A., Alsaedi, A., Waqas, M., Yasmeen, T., (2016). "Chemically reactive flow of third grade fluid by an exponentially convected stretching sheet", *Journal of Molecular Liquids*, 223: 853-860.
23. Gangaiah, T., Saidulu N. and Lakshmi, A. V., (2018). "Magnetohydrodynamic flow of nanofluid over an exponentially stretching sheet in presence of viscous dissipation and chemical reaction", *Journal of Nanofluids*, 7(3): 439-448.
24. Choi, S. U. S., (1995). "Enhancing thermal conductivity of fluids with nanoparticles", in *Proceedings of the ASME, International Mechanical Engineering Congress and Exposition*, 66, 995, San Francisco, USA.
25. Masuda, H., Ebata, A., Teramae, K., Hishinuma, N., (1993). "Alteration of thermal conductivity and viscosity of liquid by dispersing ultra-fine particles", *Netsu Bussei*, 7: 227-233.
26. Buongiorno, J., (2006). "Convective transport in nanofluids", *Journal of Heat Transfer*, 128: 240-250.
27. Nield, D. A., Kuznetsov, A. V., (2009) "The Cheng-Minkowycz problem for natural convective boundary layer flow in a porous medium saturated by a nanofluid", *International Journal of Heat and Mass Transfer*, 52(25-26): 5792-5795.
28. Angayarkanni, S. A., Philip, J., (2015). "Review on thermal properties of nanofluids: Recent developments", *Advances in Colloid and Interface Science*, 225: 146-176.
29. Sheikholeslami, M., Mollabasi, H., Ganji, D. D., (2015). "Analytical investigation of MHD Jeffery-Hamel nanofluid flow in non-parallel walls", *International Journal of Nanoscience and Nanotechnology*, 11(4): 241-248.
30. Reddy, C.S., Naikoti, K., (2016). "MHD boundary layer flow of Casson nanofluid over a non linear stretching sheet with viscous dissipation and convective condition", *Journal of Nanofluids*, 5(6): 870-879.
31. Ramya, D., Srinivasa Raju, R., Anand Rao, J., Rashidi, M. M., (2016). "Boundary layer viscous flow of nanofluids and heat transfer over a nonlinearly isothermal stretching sheet in the presence of heat generation/absorption and slip boundary conditions", *International Journal of Nanoscience and Nanotechnology*, 12(4): 251-268.
32. Casson, N., (1959). "A Flow Equation for Pigment-Oil Suspensions of the Printing Ink Type. In: Mill, C.C., Ed., *Rheology of Disperse Systems*", Pergamon Press, Oxford, 84-104.
33. Dash, R. K., Mehta, K. N., Jayaraman, G., (1996). "Casson fluid flow in a pipe filled with a homogeneous porous medium", *International Journal of Engineering Science*, 34: 1145-1156.
34. Fredrickson, A. G., (1964). "Principles and Applications of Rheology". Prentice-Hall, Englewood Cliffs.
35. Charm, S., Kurland, G., (1965). "Viscometry of human blood for shear rates of 0-100,000 sec⁻¹", *Nature*, 206: 617-618.

36. Walwander, W. P., Chen, T. Y., Cala, D. F., (1975). "An approximate Casson fluid model for tube flow of blood", *Biorheology*, 12: 111-119.
37. Malik, M. Y., Naseer, M., Nadeem, S., Rehman, A., (2014). "The boundary layer flow of Casson nanofluid over a vertical exponentially stretching cylinder", *Applied Nanoscience*, 4: 869-873.
38. Prabhakar, B., Shankar, B., (2015). "Mixed convection MHD flow of a Casson nanofluid over a non linear permeable stretching sheet with viscous dissipation", *Journal of Applied Mathematics and Physics*, 3: 1580-1593.
39. Arthur, E. M., Seini, I. Y., Bortteir, L. B., (2015). "Analysis of Casson fluid flow over a vertical porous surface with chemical reaction in the presence of magnetic field", *Journal of Applied Mathematics and Physics*, 3: 713-723.
40. Raju, C. S. K., Sandeep, N., Sugunamma, V., Babu, M. J., Reddy, J. V. R., (2016). "Heat and mass transfer in magnetohydrodynamic Casson fluid over an exponentially permeable stretching surface", *Engineering Science and Technology, an International Journal*, 19: 45-52.
41. Anantha Kumar, K., Ramana Reddy J. V., Sandeep, N., Sugunamma, V., (2016). "Dual solutions for thermo diffusion and diffusion thermo effects on 3D MHD Casson fluid flow over a stretching surface", *Research Journal of Pharmacy and Technology*, 9(8): 1187-1194.
42. Tamoor, M., Waqas, M., Ijaz Khan, M., Alsaedi, A., Hayat, T., (2017), "Magnetohydrodynamic flow of Casson fluid over a stretching cylinder", *Results in Physics*, 7: 498-502.
43. Pramanik, S., (2014). "Casson fluid flow and heat transfer past an exponentially porous stretching surface in presence of thermal radiation", *Ain Shams Engineering Journal*, 5: 205-212.
44. Hayat, T., Ashraf, M. B., Shehzad, S. A., Alsaedi, A., (2015). "Mixed convection flow of Casson nanofluid over a stretching sheet with convectively heated chemical reaction and heat source/sink", *Journal of Applied Fluid Mechanics*, 8(4): 803-813.
45. Bhattacharyya K., Uddin, M. S., Layek, G. C., (2016). "Exact solution for thermal boundary layer in Casson fluid flow over permeable shrinking sheet with variable wall temperature and thermal radiation" *Alexandria Engineering Journal*, 55: 1703-1712.
46. Anki Reddy, P. B., (2016). "Magnetohydrodynamic flow of a Casson fluid over an exponentially inclined permeable stretching surface with thermal radiation and chemical reaction", *Ain Shams Engineering Journal*, 7: 593-602.
47. Kumar, P. V., Ibrahim, S. M., Lorenzini, G., (2017). "Computational modeling of magnetohydrodynamic Casson nanofluid flow over an exponentially slendering surface with radiation and heat Source", *International Journal of Emerging Engineering Research and Technology*, 5: 1-12.
48. Zaigham Zia, Q. M., Ikram, U., Waqas, M., Alsaedi, A., Hayat, T., (2018), "Cross diffusion and exponential space dependent heat source impacts in radiated three-dimensional (3D) flow of Casson fluid by heated surface", *Results in Physics*, 8: 1275-1282.
49. Lakshmi, K. B., Kumar, K. A., Reddy, J. V. R., Sugunamma, V., (2019). "Influence of nonlinear radiation and cross diffusion on MHD flow of Casson and Walters-B nanofluids past a variable thickness sheet", *Journal of Nanofluids*, 8(1): 73-83.
50. Sparrow, E. M., Cess, R. D., (1978). "Radiation Heat Transfer", Hemisphere, Washington, USA.
51. Brewster, M. Q., (1992). "Thermal Radiative Transfer and Properties", John Wiley and Sons, New York, USA.
52. Dulal Pal, (2010). "Mixed convection heat transfer in the boundary layers on an exponentially stretching surface with magnetic field", *Applied Mathematics and Computation*, 217(6): 2356-2369.